Supporting information

Precision-Engineered, Polymer-Lean, Digital Light Processing 3D-printed Hydrogels for Enhancing Solar Steam Generation and Sustainable Water Treatment

S. Mao,[1] X. Zhang,[1] Y. Shi,[1] A. Feng,[1] C. Onggowarsito,[1] X. Xu,[2] L. Aditya,[1] Y.Sun,[3]* L. Nghiem,[1]* and Q. Fu[1]*

1. Centre for Technology in Water and Wastewater, School of Civil and Environmental Engineering, University of Technology Sydney, Ultimo 2007, NSW, Australia

2. School of Biomedical Engineering, University of Technology Sydney, Ultimo 2007, NSW, Australia

3. School of Materials Science and Technology, North University of China, Taiyuan, People's Republic of China

Corresponding to Q. Fu, Qiang.fu@uts.edu.au; L. Nghiem, duclong.nghiem@uts.edu.au; Y. Sun, syyi@pku.edu.cn

Table of Contents

S1. Supplementary Figures and Tables

S2. Supporting references

S1. Supplementary Figures and Tables

S1.1 The development of 3D printing ink.

Table S1. The development of 3D printing ink for DLP. The concentration of GO is the same in all formulations (0.5 mg mL^{-1}).

Monomer	**Crosslinker**	**Photo-initiator**	**Solvent and additives**	**Comments**
8.75 g Poly(ethylene glycol) diacrylate Mn 575 (PEGDA 575)		4 g 2,4,6-trimethylbenzoyldiphenyl phosphine oxide (TPO)	15.25 g Ethanol	Printing was possible, but cracked when contacting water due to differences in solvent surface tension, not suitable for long-time SSG application.
10 g PEGDA 575		75 mg LAP	30 mL Water	Printing was possible, but could not print fine structures.
7.34 g Acrylamide (AM)	111.4 mg N,N'-Methylenebisacrylamide (bis)	75 mg LAP	30 mL Water	Printing failed. Hydrogel swelling during the printing caused wrinkling and detachment from the printing platform.
9.79 g AM	148.5 mg N,N'-Methylenebisacrylamide (bis)	75 mg LAP	30 mL 5 wt% PVA aqueous solution	Printing failed. The hydrogel was too sticky, leading to failure in separating from the release film.
7.5 g Poly(ethylene glycol) dimethacrylate Mn 550		75 mg LAP	30 mL Water	Printing was possible, but had a weak affinity with GO, resulting in a white printed hydrogel.
10 g Poly(ethylene glycol) methyl ether	100 mg PEGDA 575	75 mg LAP	30 mL Water	Printing failed. Took more than 2 minutes to crosslink one layer.

methacrylate Mn 500				
10 g Poly(ethylene glycol) methyl ether acrylate M_n = 480	150 mg Bis or PEGDA 575	75 mg LAP	30 mL Water	Printing successfully, but easily to break after swelling in water.
10.0 g Poly(ethylene glycol) methyl ether acrylate Mn 480 and 2.5 g AM	125.0 mg Bis	75 mg LAP	30 m L Water	Printing successfully, but too soft, not suitable for long-time SSG application.
16.974 g N-Isopropylacrylamide and 1.81 g AM	30 mg PEGDA 575	75 mg LAP	30 mL Water	Printing failed.
5 g Poly(ethylene glycol) dimethacrylate M_n = 550, 2.5 g Poly(ethylene glycol) methyl ether acrylate Mn 480, and 2.5 g AM		100 mg LAP	40 mL Water	Printing successfully, but fragile.
5.94 g Diacetone acrylamide	60 mg PEGDA 575	60 mg LAP	24 mL Water	Printing failed. The hydrogel was too sticky, leading to failure in separating from the release film. The hydrogel had a weak affinity with GO, resulting in a white printed hydrogel.

Supplementary Note 1

We encountered several challenges and did not achieve satisfactory printing results. For instance, we tried to prepare printing ink containing monomer acrylamide (AM) and cross-linker *N,N′*-methylenebisacrylamide (MBA). However, we observed that the printed hydrogel parts swelled excessively during repeated immersions into the ink and then detached from the printing platform midway through the print run. Although printing can be achieved using a formulation based on poly(ethylene glycol) methyl ether acrylate (PEGMA, $M_n = 480$ g mol^{-1}) and polyethylene glycol diacrylate (PEGDA, $M_n = 575$ g mol^{-1}), the resulting hydrogels exhibit insufficient mechanical strength and are prone to cracking under the swelling force of water, rendering them unsuitable for SSG applications.

Instead of using post-treatment to incorporate photothermal materials into the 3D-printed hydrogels, directly adding graphene oxide (GO) to the printing formulation introduced several challenges. Certain cross-linker, such as poly(ethylene glycol) dimethacrylate (PEGDMA, $M_n = 550$ g mol^{-1}), exhibited weak affinity with GO, resulting in printed hydrogels appearing white, indicating limited GO incorporation. Additionally, the GO concentration needed to remain low to prevent excessive UV light absorption, which could interfere with LAP activation. As shown in Supplementary reference S4, a higher concentration of oxidized carbon black was used, necessitating a significant increase in photo-initiator usage for compensation, which also raised the overall cost. We meticulously regulated our GO concentration to 0.5 mg mL^{-1} in all formulations to reduce the cost as well as maintain the light adsorption.

Table S2. Dimensional parameters and calculated printing accuracy of 5PVA15PHEA-C.

Dimensional parameters	**Designed size** mm	**Printed size** mm	**Printing accuracy** %
Diameter	25	25	100
Thickness	10	9	90
Hole’ s diameter	2	1.9	95

Table S3. Dimensional parameters and calculated shrinkage ratio of 5PVA15PHEA-C.

Dimensional parameters	**Freeze-dried sample** mm or mm^3	**Well-saturated sample** mm or mm^3	**Shrinkage** %
Diameter	22	25	12%
Thickness	6	9	33.3%
Volume	2280.8	4417.9	48.4%

S 1.2 The morphology of 3D printed hydrogels with 25 wt% precursors loading

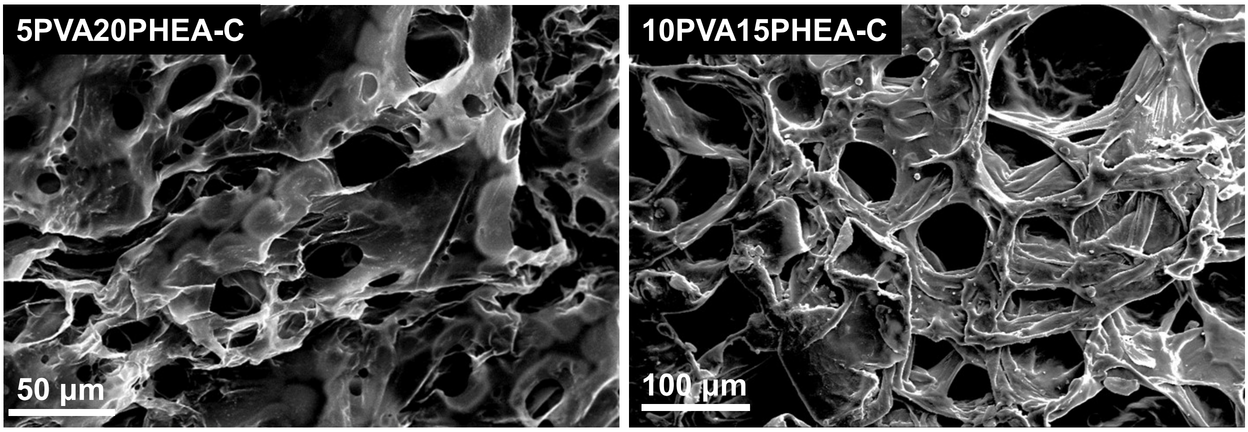

Figure S1. The SEM images of the pore structure in the concave 3D printed hydrogel of 5PVA20PHEA-C and 10PVA15PHEA-C, respectively.

Supplementary Note 2

At higher precursor concentration loadings, fewer pores were formed, and the internal pores tended to be more disordered. This resulted in thicker pore walls and lower porosity, which hinder water transport and affect the interactions between the polymer chains and water. The SEM images below show a cross-sectional view highlighting a region where more pores can be observed.

S 1.3: The pore size of the 3d printed hydrogels

Table S4. The average pore size of the 3d printed hydrogels calculated from the SEMs via Imagej.

Sample	Average pore size (μm)
5PVA15PHEA-C	21.9
5PVA15PHEA-N	17.5
5PVA15PHEA-H	19.8
5PVA20PHEA-C	16.2
10PVA15PHEA-C	59.9

S1.4 FT-IR spectra of printed hydrogels with 25 wt% precursors loading.

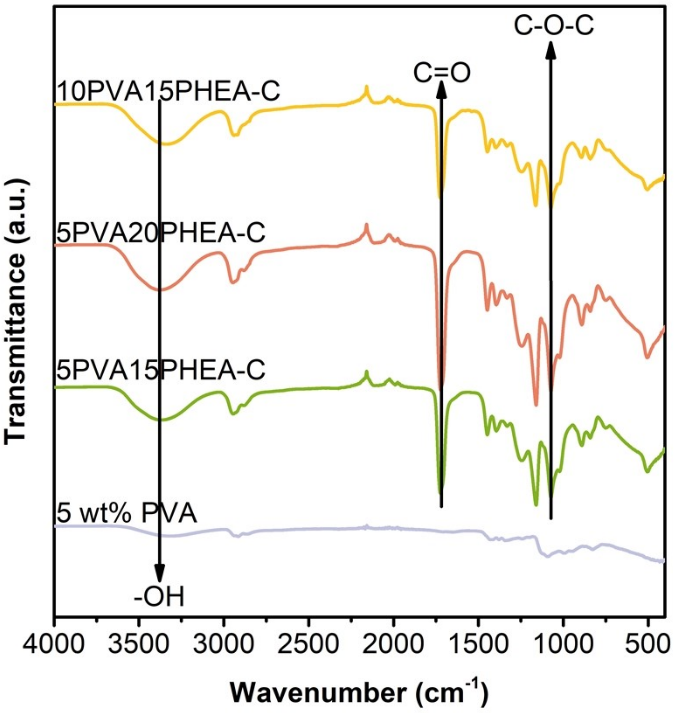

Figure S2. FT-IR spectra of the 5PVA15PHEA-C, 5PVA20PHEA-C, and 10PVA15PHEA-C hydrogels. The control sample is a pristine 5 wt% PVA hydrogel directly crosslinked with GA.

S1.5 Model and printed hydrogels

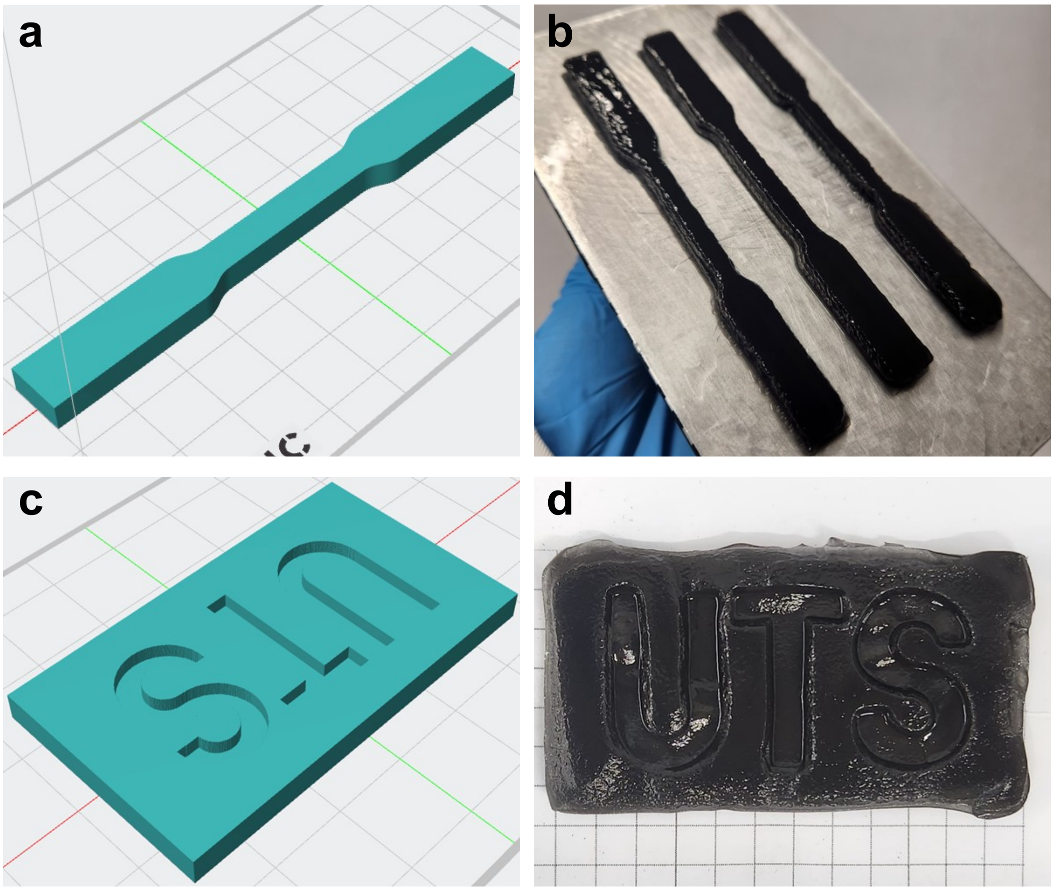

Figure S3. (a) The 3D model of ASTM (E8) subsize standard hydrogel specimen for tensile test, and (b)the 3D printed hydrogels from the model. (c) The 3D model of “UTS” concave patterns, and (d) the 3D printed hydrogels from the model.

S1.6 Contact angle test.

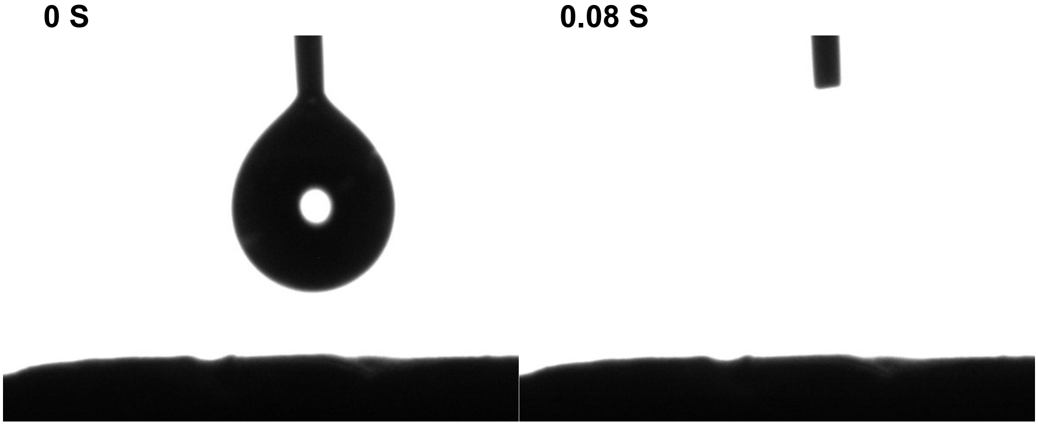

Figure S4. The contact angle test of 3D printed 5PVA15PHEA hydrogel.

S1.7 Temperature variations of printed hydrogels with 25 wt% precursors loading

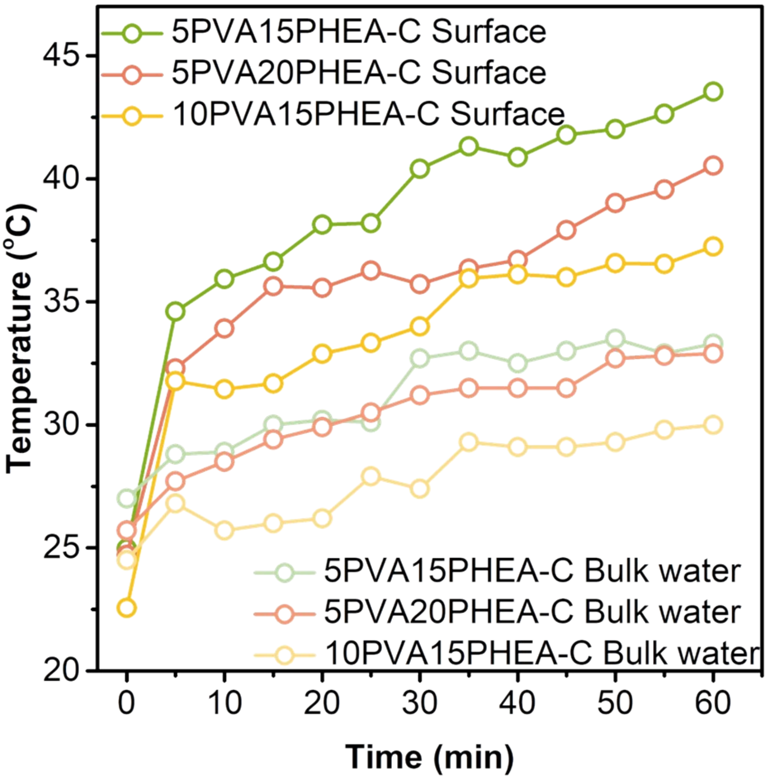

Figure S5. The temperature variations of the 5PVA15PHEA-C, 5PVA20PHEA-C, and 10PVA15PHEA-C hydrogel surfaces and bulk water during the SSG test under one sun irritation.

S1.8 Water uptake in printed hydrogels with 25 wt% precursors loading

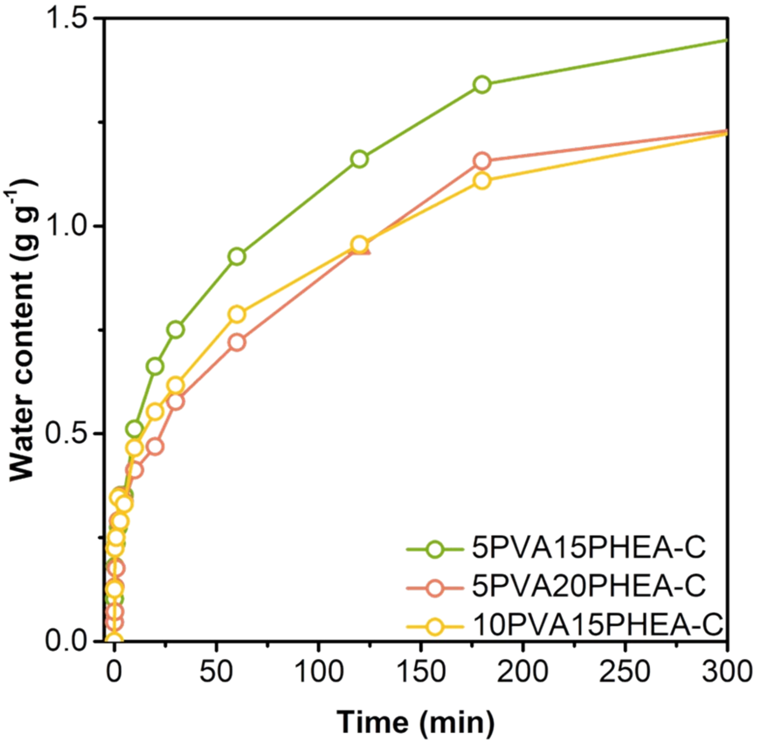

Figure S6. The water content vs absorption time of 3D printed hydrogels. The unit is measured gram of water per gram of dry gel.

S1.9 Evaporation rates of printed hydrogels with 25 wt% precursors loading

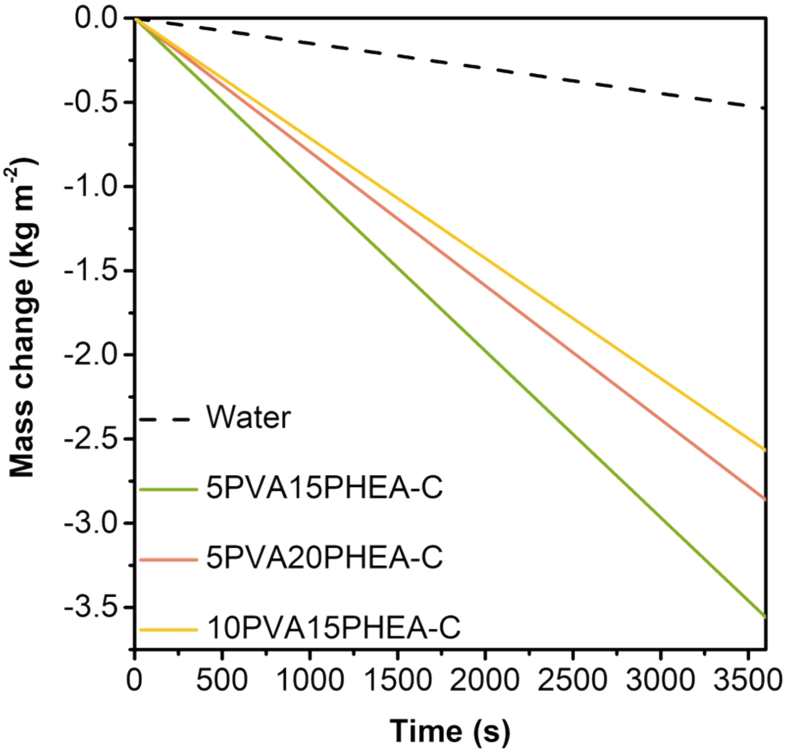

Figure S7. Water mass changes under one sun irritation condition for 5PVA15PHEA-C, 5PVA20PHEA-C, and 10PVA15PHEA-C hydrogels, respectively (in DI water).

S1.10 Raman spectra and the fitting curves to calculate intermediate water content

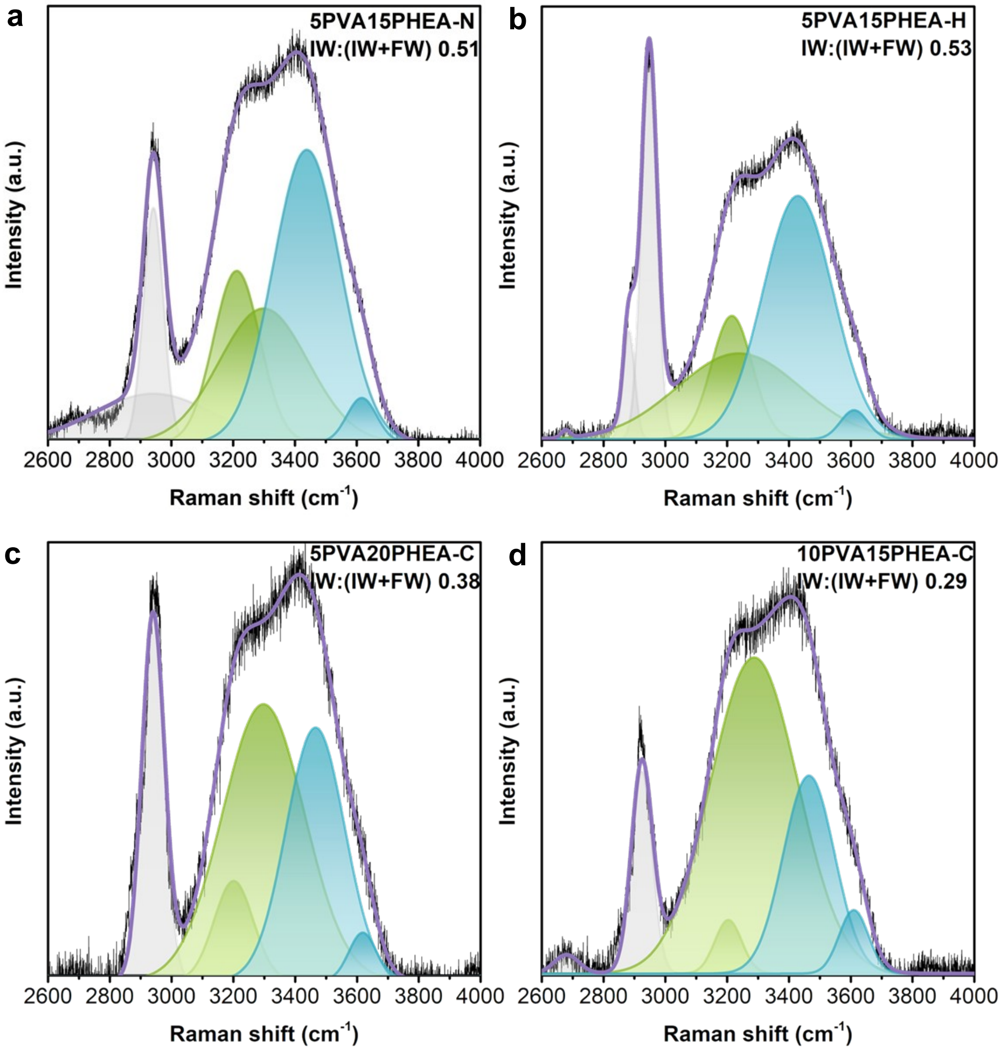

Figure S8. Fitting curves for the a) 5PVA15PHEA-N, b) 5PVA15PHEA-H, c) 5PVA20PHEA-C, and d) 10PVA15PHEA-C hydrogels in the Raman spectra within the O-H stretching energy region. Free water is indicated by the green peaks, whereas intermediate water by blue peaks.

Supplementary Note 3

Intermediate water (IW) refers to water molecules characterized by weaker or partially formed hydrogen bonds, positioned between those directly that are directly associated with polymer chains (*aka.* bound water, BW) and those that do not interact with the polymer chains (*aka.* free water, FW). Due to the weaker bonding, IW molecules exhibit a greater tendency to dissociate from neighboring molecules. The IW content can be quantified by Raman measurements. The presence of IW molecules, characterized by weaker or partially formed hydrogen bonds, is indicated by the blue peaks at approximately 3,514 cm^{-1} and 3,630 cm^{-1}. In contrast, the green peaks at 3,233 cm^{-1} and 3,401 cm^{-1} correspond to FW with fully formed hydrogen bonds.

S1.11 Differential scanning calorimetry (DSC) curves

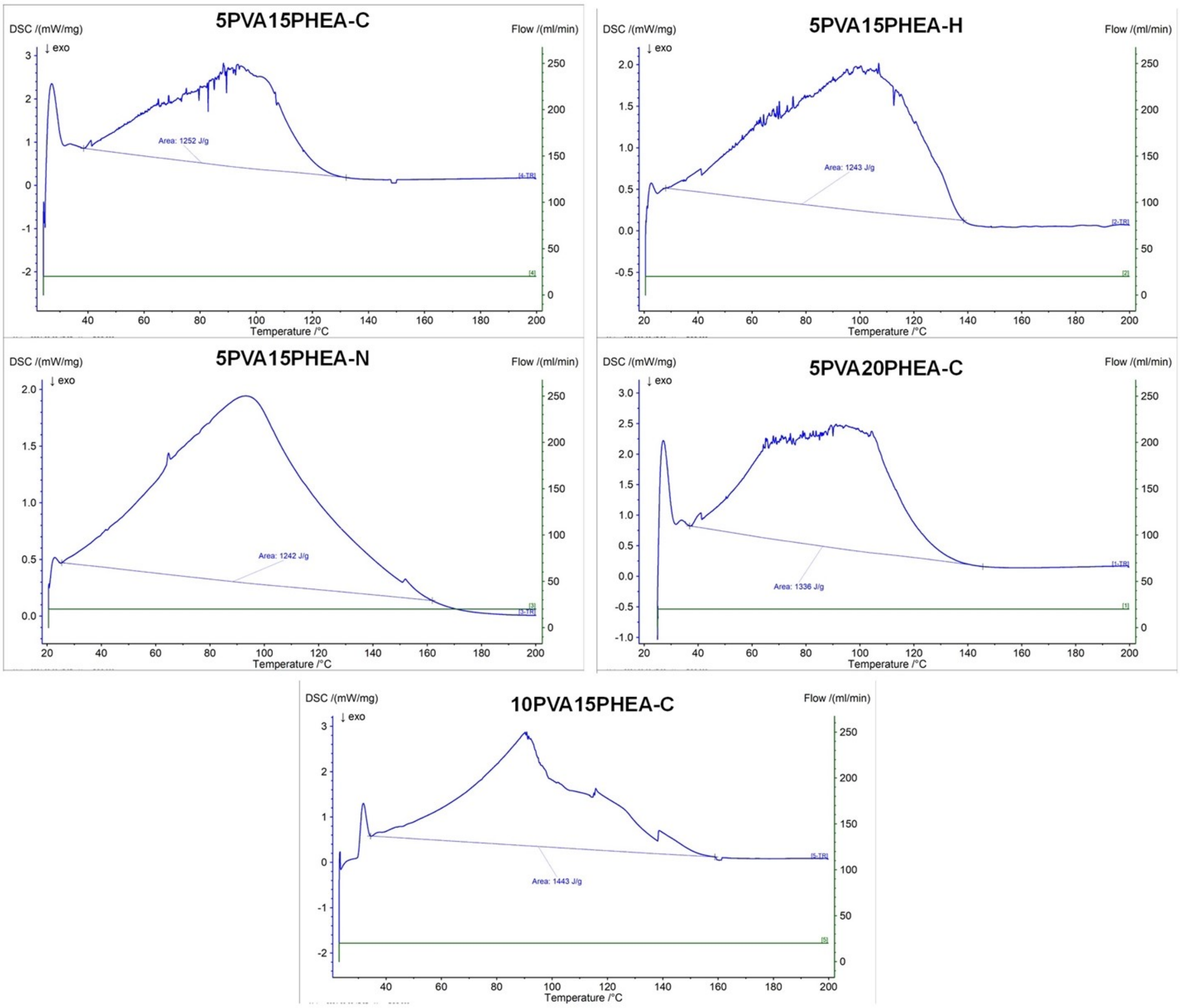

Figure S9. Raw DSC curves and the equivalent water vaporization enthalpies calculated from the integrated area of 5PVA15PHEA-C, 5PVA15PHEA-N, 5PVA15PHEA-H, 5PVA20PHEA-C, and 10PVA15PHEA-C hydrogels, respectively.

Supplementary Note 4

Differential scanning calorimetry (DSC) is used to measure the vaporization energy of water in the printed hydrogels, demonstrating the reduction in water's evaporation enthalpy within these hydrogels. Figure S9 shows the change of heat flow signal as a function of temperature, and the equivalent water vaporization enthalpies can be calculated from the integrated area.

S1.12 Prior studies employing DIP and DIW 3D printing for SSG

Table S5. Evaporation rates and polymer mass loading of the DLP 3D printed hydrogels from previous work.

Ref.	**Polymer mass loading** wt%	**Evaporation rate** kg m^{-2} h^{-1}
S1	57.3	2.78
S2	25.0	2.85
S3	44.8	2.96
S4	47.6	3.59
S5	27.0	3.14
S6	91.0	2.41
This work	**20.0**	**3.56**

Table S6. Evaporation rates and polymer mass loading of the DIW 3D printed hydrogels from previous work.

Ref.	**Polymer mass loading** wt%	**Evaporation rate** kg m^{-2} h^{-1}
S7	30.4	1.33
S8	11.7	3.23
S9	20.0	2.13
S10	2.5	2.90
S11	10.0	2.62
This work	**20.0**	**3.56**

S1.13 5PVA15PHEA-C, N, and H hydrogels after 6 hours of SSG tests in seawater

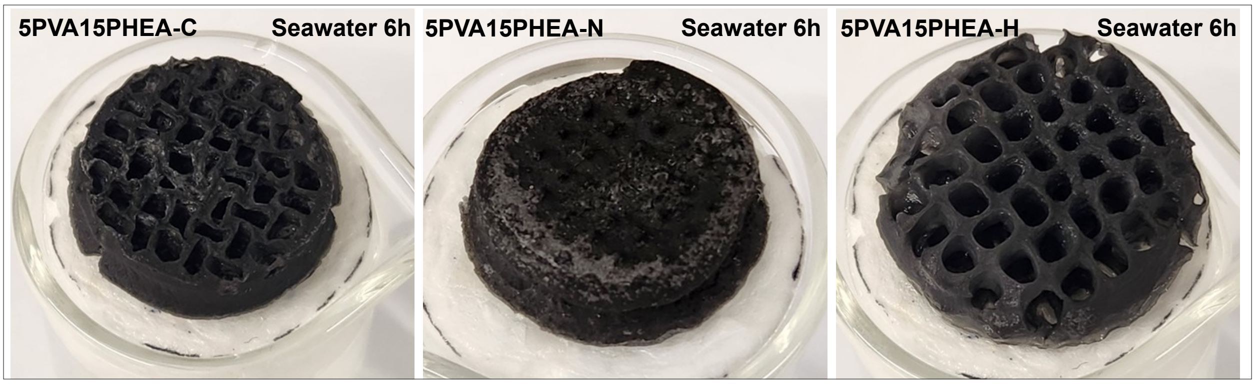

Figure S10. The physical images of 5PVA15PHEA-C, N, and H hydrogels after 6 hours of SSG tests in seawater.

S1.14 The anti-salting-out property of the 3D printed hydrogels

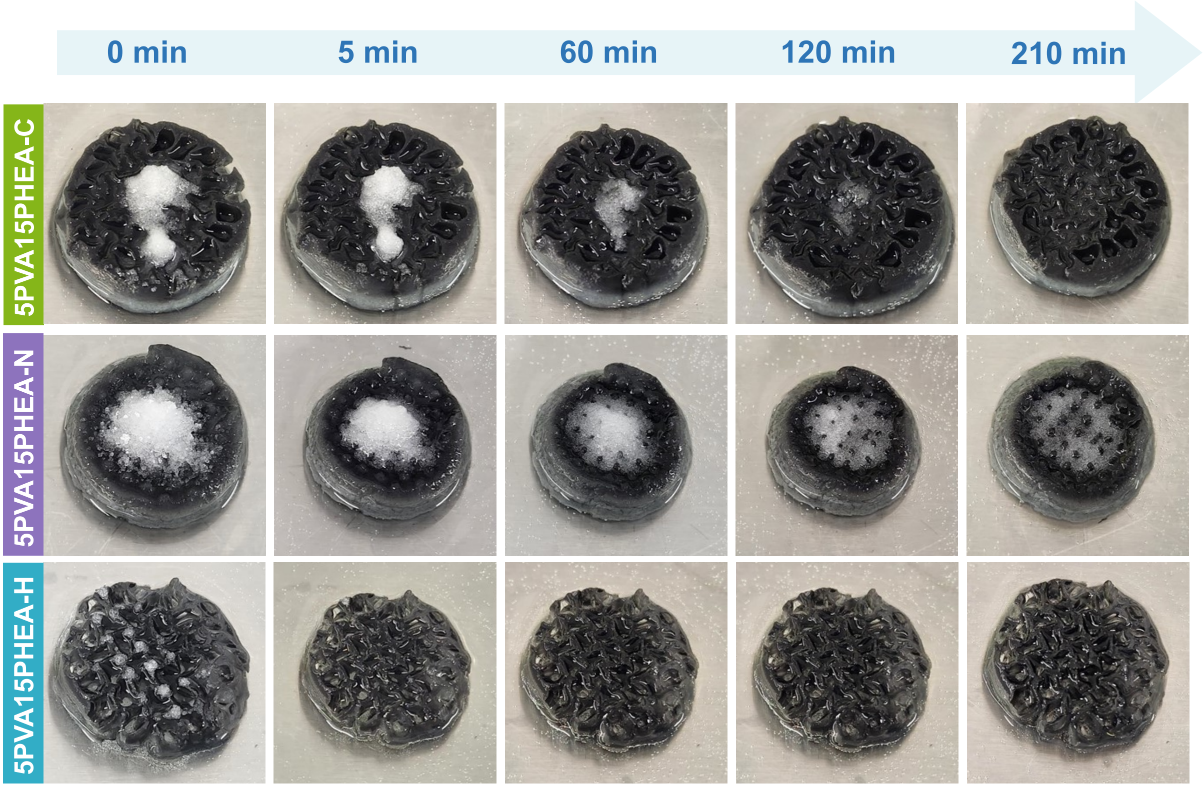

Figure S11. The physical images of self-desalting behavior of 5PVA15PHEA-C, N, and H hydrogels.

Supplementary Note 5

0.5 g of NaCl was placed on the surface of each hydrogel. The 5PVA15PHEA-H hydrogel rapidly dissolved the surface salt within 5 minutes, facilitated by efficient water transported via capillary action through its through-pores. In comparison, The 5PVA15PHEA-C dissolved the salt entirely in around 200 minutes, assisted by the Marangoni effect due to its concave structure. Conversely, the 5PVA15PHEA-N hydrogel retained some salt, attributed to its relatively limited water transport capability.

S1.15 The sealed jar to collect condensate.

Figure S12. The sealed jar to condense and collect purified seawater or water with dye.

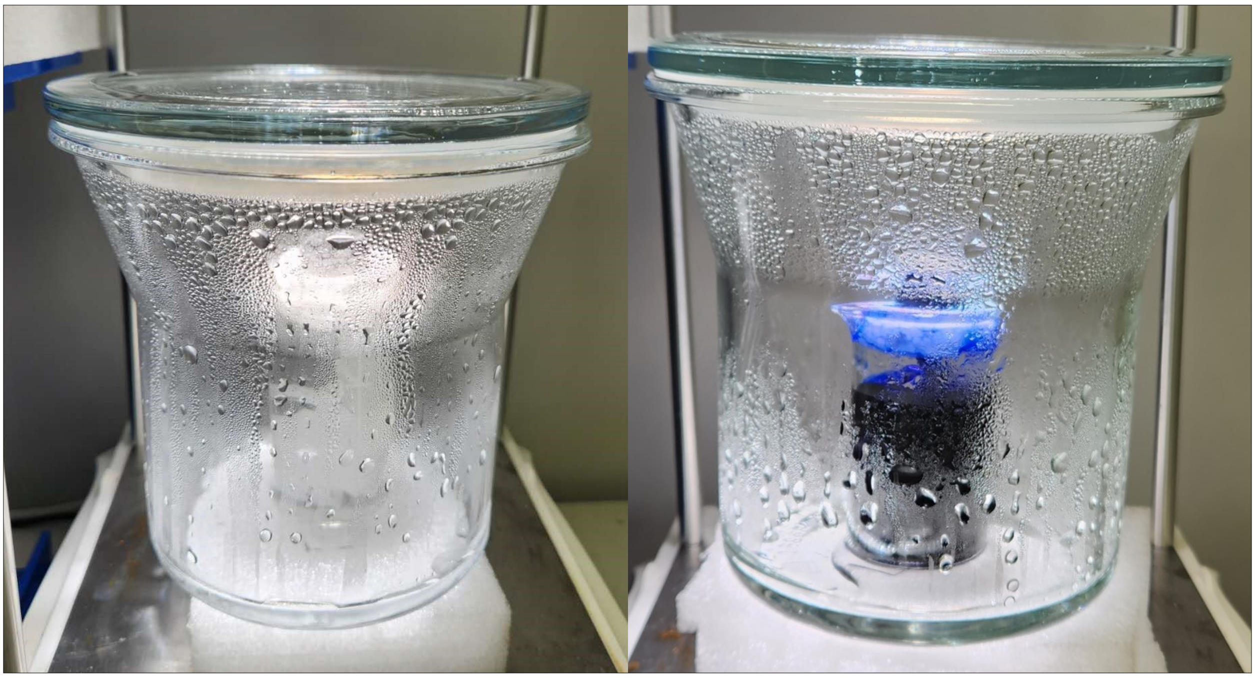

S1.16 Larger 3D printed hydrogels

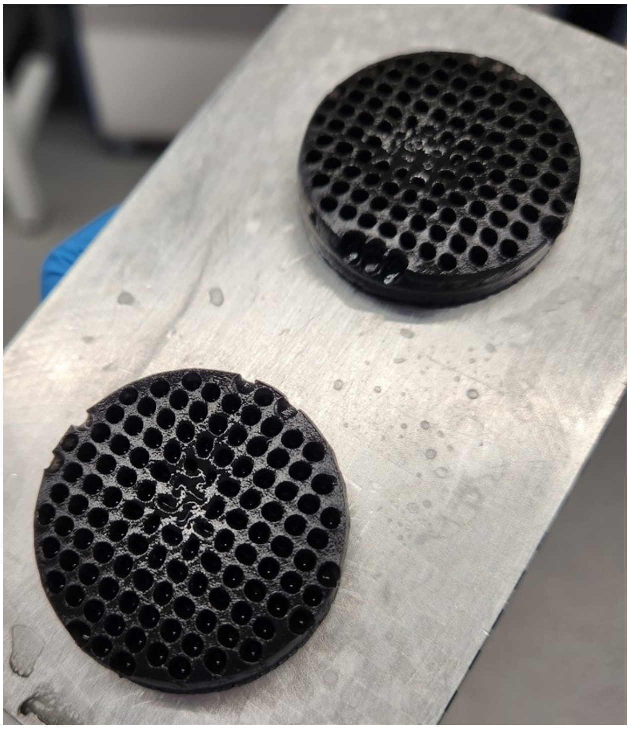

Figure S13. Physical image of the 3D printed larger 5PVA15PHEA-C hydrogels (with a diameter of 4 cm) for outdoor SSG.

S1.17 Custom-designed outdoor SSG device

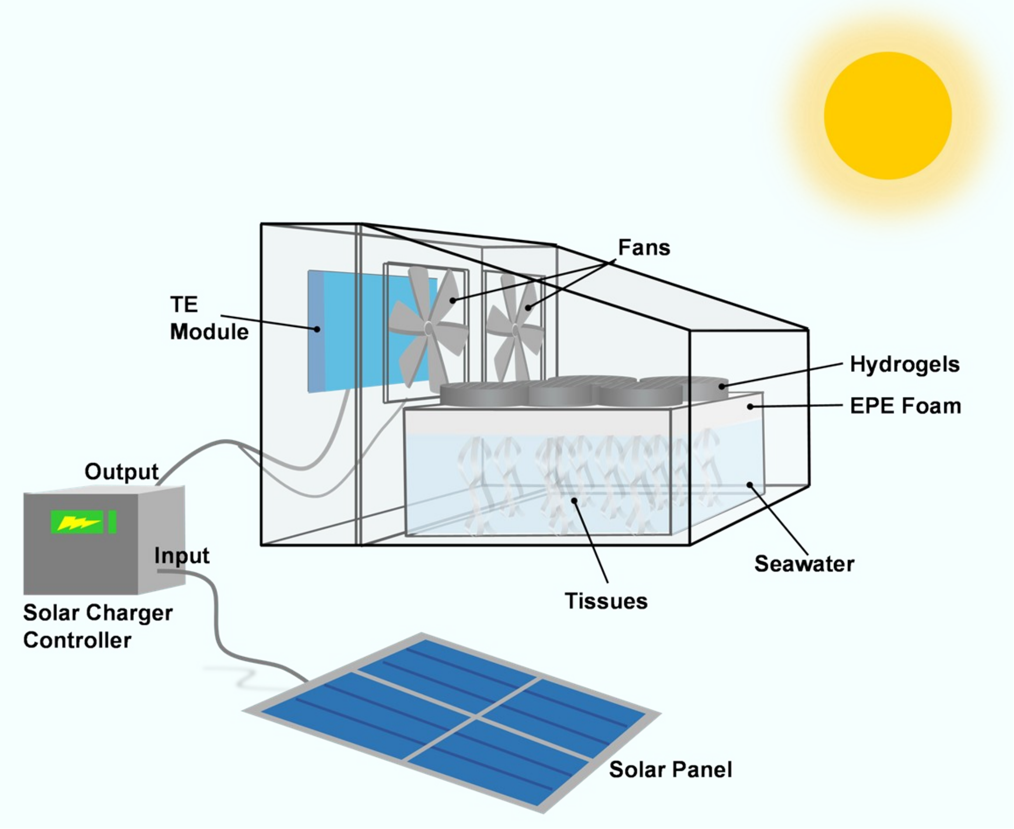

Figure S14. Schematic illustration of the home-made outdoor solar steam generation device.

Supplementary Note 6

To enhance condensation efficiency and increase freshwater productivity, our outdoor device design separates the evaporation chamber from the condensation chamber, as an integrated single-chamber setup cannot simultaneously achieve the high temperatures needed for evaporation and the low temperatures needed for condensation. An acrylic sheet was used to partition the chambers, with two fans embedded to transport generated steam to the condensation chamber. Two thermoelectric (TE) modules effectively cool down the steam as it is directed by the fans. The hydrogels, fans, and cooling side are positioned on the same horizontal plane, facilitating a larger volume of vapor transfer to the condensation chamber for prompt condensation. Additionally, the independent seawater evaporation chamber condenses vapor along its perimeter due to the lower temperature of the seawater, allowing for easy collection of any vapor that is not transferred to the condensation chamber. The TE modules, fans, and water-cooling pump are powered by a Powertech Portable 155W Power Centre as the charge controller, which is supplied in real-time by a 12V 10W solar panel to ensure no extra ennergy input in our system.

S2. Supporting references

S1. X. Zheng, Y. Bao, A. Huang, G. Qin and M. He, *Separation and Purification Technology*, 2023, **306**, 122741.

S2. Z. Sun, Q. Zhao, S. Ma and J. Wu, *Mater Horiz*, 2023, **10**, 179-186.

S3. S. Yang, H. Zhang, X. Sun, J. Bai and J. Zhang, *ACS Nano*, 2024, **18**, 5847-5863.

S4. Y. Liu and X. Zheng, *Solar Energy*, 2024, **273**, 112507.

S5. Z. Zhan, L. Chen, C. Wang, Y. Shuai, H. Duan and Z. Wang, *ACS Appl Mater Interfaces*, 2023, **15**, 8181-8189.

S6. Y. Xiao, B. Liu, D. Li, X. Zheng, J. Li and G. Qin, *Chemical Engineering Journal*, 2024, **497**, 155038.

S7. J. Yuan, X. Lei, C. Yi, H. Jiang, F. Liu and G. J. Cheng, *Chemical Engineering Journal*, 2021, **430**, 132765.

S8. B. Huang, R. Tang, X. Zheng, G. Chen, Q. Li, W. Zhang and B. Peng, *Journal of Environmental Chemical Engineering*, 2024, **12**, 111827.

S9. S. Zhang, M. Li, C. Jiang, D. Zhu and Z. Zhang, *Advanced Science*, 2024, **11**, 2308665.

S10. N. Li, K. Shao, J. He, S. Wang, S. Li, X. Wu, J. Li, C. Guo, L. Yu and P. Murto, *Small*, 2023, **19**, 2301474.

S11. Y. Liu, B. Luo, H. Liu, M. He, R. Wang, L. Wang, Z. Quan, J. Yu and X. Qin, *Chemical Engineering Journal*, 2023, **452**, 139402.